Electron-impact dissociation of CH_2^+ ions: Measurement of CH^+ and C^+ fragment ions

C. R. Vane,* E. M. Bahati, and M. E. Bannister
Physics Division, Oak Ridge National Laboratory, Oak Ridge, Tennessee 37831-6372, USA

R. D. Thomas
Department of Physics, Albanova, Stockholm University, SE106 91 Stockholm, Sweden
(Received 19 March 2007; published 22 May 2007)

Absolute cross sections for electron-impact dissociation of CH_2^+ producing CH^+ and C^+ fragment ions were measured in the 3–100 eV range using a crossed electron-ion beams technique with total uncertainties of about 11% near the cross section peak. The cross sections are nearly identical for energies above 15 eV, but they are dramatically different at lower energies. The CH^+ channel exhibits a strong peak rising from an observed threshold of about 6 eV; the C^+ channel is relatively flat down to the lowest measured energy. Ionization cross sections for the CH_2^+ ion are also presented.

DOI: 10.1103/PhysRevA.75.052715 PACS number(s): 34.80.Kw, 34.80.Ht

I. INTRODUCTION

In many low-temperature plasma environments, collisions of electrons with molecular ions play an important role in the chemistry, particle and energy balance, and neutral transport. In particular, abundant and diverse hydrocarbon ions are found in the divertor and edge plasmas of fusion devices that use graphite for plasma-facing components [1] and may contribute to detachment of divertor plasmas through molecule assisted recombination [2]. Hydrocarbon ions are also important in the chemistry of diffuse interstellar and planetary clouds [3] and in the plasma processing of diamond films [4,5]. Hence, cross sections for interactions of these molecular ions with electrons, atoms, and photons are vital for modeling and diagnosing a variety of plasma environments.

The production of CH^+ fragment ions by electron-impact dissociation of CH_2^+ ions can proceed via a number of different channels as given in Table I along with thresholds given by Janev and Reiter [6]. The first process, direct dissociative excitation (DDE), involves a vertical transition from the initial state of CH_2^+ to a dissociative excited state. Another pathway of DDE involves a vertical transition to an excited but bound state that then couples to a dissociative state. The second process, resonant dissociative recombination (RDE), proceeds through the resonant capture of the incident electron to a Rydberg state of the neutral molecule CH_2^{**} which then decays by ejecting an electron and dissociating. Thresholds for RDE are not given by Janev and Reiter [6] for CH_2^+ ions, but we expect that they are less than for the DDE process as is the case for CH^+ ions [6]. Hereafter, we will refer to the first two processes together as simply dissociative excitation (DE). Dissociative ionization (DI), the third process, is similar to DDE but ends in a dissociative state with two ion fragments. Although not shown in Table I, it is also possible for DI to proceed through ionization to form CH_2^{2+}, which then dissociates giving fragment ions like the more direct DI processes. Another process producing CH^+ and C^+ fragments, resonant ion pair (RIP) formation, is expected to be negligible compared to the DE and DI contributions, based on RIP measurements on other similar systems [7–9]. The dissociation of CH_2^+ producing C^+ ions involves the same processes, but there are more channels available since fragmentation with H_2 or H_2^+ products is also possible, as given in Table I. In the present measurements coincidentally ejected light-mass fragments (H, H^+, H_2, or H_2^+) are not detected.

The electron-impact dissociation of CH_2^+ and CD_2^+ in the light-ion-fragment DE channels has been investigated previously using two different techniques. Djurić *et al.* [10] measured the sum of DE and DI for the D^+ production channel using a crossed-beams technique. Larson *et al.* [11] investigated the same light ion fragment DE channels in CH_2^+ at the CRYRING heavy ion storage ring, although they directly detected the corresponding neutral products CH and (C+H) with solid-state surface-barrier detectors. The agreement between the two sets of measurements for the light-ion-fragment channels is excellent, suggesting that the DI contributions are small for energies measured in the CRYRING experiment (up to 55 eV). However, there have been no published measurements for dissociation of CH_2^+ producing the heavy ion fragments CH^+ and C^+. Janev and Reiter [6,12] have recently published a review of data for collisions of simple hydrocarbon ions and neutrals with electrons and protons, including empirical formulas for electron-impact DE and DI of CH_2^+, along with information about the thresholds and average kinetic energies of release (KERs) for these processes.

The measurements reported here are absolute total cross sections for the production of CH^+ and C^+ ions by electron-impact on CH_2^+. The measurements were performed using the ORNL electron-ion crossed beams apparatus [13,14] with CH_2^+ ions produced in a Caprice electron-cyclotron-resonance (ECR) ion source. Dissociation cross sections measured for heavy fragment ion channels using this apparatus have been reported for H_3O^+ and D_3O^+ [15], CH^+ [16], and DCO^+ [17]. In the absence of other experimental or theoretical data, the present results are compared with the empirical fits of Janev and Reiter [6,12].

II. EXPERIMENT

The electron-ion crossed beams apparatus used for the present study has been described in detail previously [13,14],

*Electronic address: vanecr@ornl.gov

TABLE I. Processes for electron-impact dissociation of CH_2^+ ions producing CH^+ and C^+ fragment ions. Thresholds are taken from Ref. [6] and are given in eV for CH_2^+ ions in the $v=0$ ground state. The last two DI thresholds, denoted with an asterisk, are calculated from the value of the one channel given by Ref. [6] by subtracting the energy of association for H_2^+ and adding the ionization energy of H, respectively. Resonant ion pair formation processes are not included; see text for an explanation.

Process	Channel	Threshold (eV)
Direct dissociative excitation (DDE)	$e+CH_2^+ \rightarrow e+CH^+ +H$	6.08
Resonant dissociative excitation (RDE)	$\rightarrow CH_2^{**} \rightarrow e+CH^+ +H$	
Dissociative ionization (DI)	$\rightarrow e+CH^+ +H^+ +e$	30.41
Direct dissociative excitation (DDE)	$e+CH_2^+ \rightarrow e+C^+ +H_2$	5.62
	$\rightarrow e+C^+ +H+H$	11.52
Resonant dissociative excitation (RDE)	$\rightarrow CH_2^{**} \rightarrow e+C^+ +H_2$	
	$\rightarrow CH_2^{**} \rightarrow e+C^+ +H+H$	
Dissociative ionization (DI)	$\rightarrow e+C^+ +H^+ +H+e$	34.15
	$\rightarrow e+C^+ +H_2^+ +e$	31.48*
	$\rightarrow e+C^+ +H^+ +H^+ +2e$	47.74*

and recent modifications and issues specific to measurements of cross sections for dissociation of molecular ions have also been published [16,17], so the discussion here will be abbreviated. The apparatus is shown schematically in Fig. 1.

A. Crossed-beams method

The CH_2^+ molecular ions were produced in the ORNL ECR ion source [18] using methane as a source gas. The ions were extracted at 10 kV and mass selected with magnetic analysis, and then transported with magnetic and electrostatic optics from the ECR ion source to the crossed beams apparatus. Just before the collision volume the ions are deflected electrostatically through 90° in a charge purifier to eliminate any charge-exchange components in the beam. In the collision volume, the ion beam (1 mm diameter) interacts at a right angle with an electron beam formed by a magnetically confined gun described below. Upon leaving this interaction region, the parent and fragment ions are separated by a double-focusing 90° sector analyzing magnet with a radius of curvature of 20 cm. This ensures that the collision volume is imaged at the throat of the fragment ion detector. The CH^+ or C^+ product ions are selectively deflected 90° by the magnet, then electrostatically deflected out of the magnetic dispersion plane and onto a 1.0 cm diameter channel electron multiplier (CEM). For the CH^+ fragment measurements, the CH_2^+ primary ions are deflected less by the analyzing magnetic field and collected in Faraday cup 2, which is closest to the fragment ion detector (see Fig. 1). For the C^+ fragment measurements, the CH_2^+ primary ions are collected in Faraday cup 1. The post-collision Einzel lens shown in Fig. 1 is grounded for all measurements reported here.

The electron gun used for the present study is a magnetically confined model described previously [14,19,20]. A magnetic field of 250 G confines the electrons and yields a uniform rectangular cross section (approximately 2 mm wide by 10 mm high) over the 2 mm length of the interaction region. Spiraling of the electrons is minimized [20] by accel-

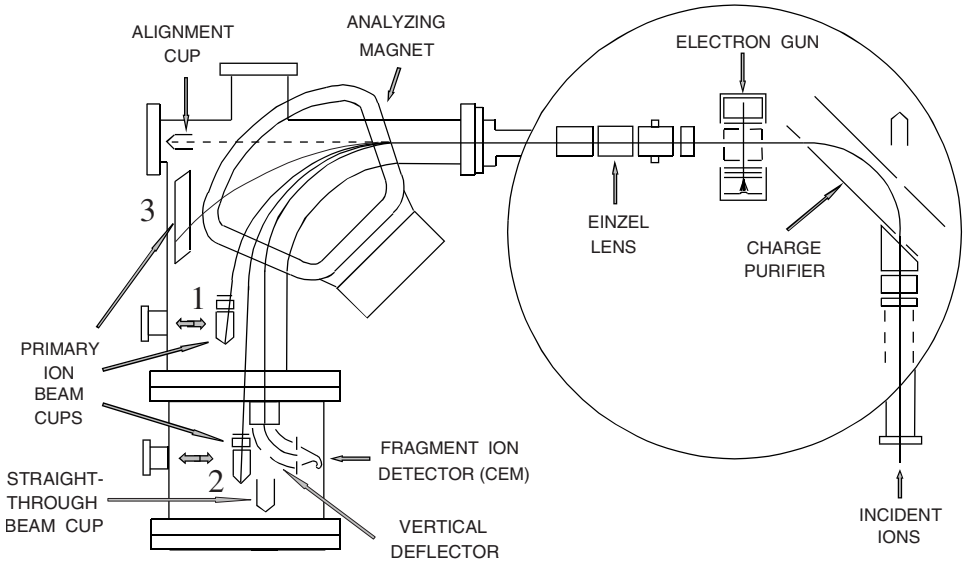

FIG. 1. Electron-ion crossed-beams experimental apparatus. See text for an explanation. The fragment ion detector and vertical deflector are rotated 90° to the plane of the figure.

erating them in a uniform electric field through a series of apertures between the indirectly heated planar cathode and the collision volume. The electron collector consists of a stack of tantalum "razor blades" turned with the sharp edges facing the interaction region; this design helps prevent backscattered electrons from returning to the collision volume. The collector is also biased +300 V with a battery to minimize the escape of secondary electrons. Typical electron currents are 11 μA at 10 eV and 230 μA at 100 eV. The electrons are chopped at 1 kHz in order to separate the dissociation signal from the relatively larger background count rate associated with the ion beam. Previous measurements [21] of excitation cross sections using the configuration shown in Fig. 1 [21] indicated that the net collision energy distribution is about 1.5 eV full width at half maximum as a result of field leakage into the collision region from post-collision ion deflector plates.

The overlap of the ion and electron beams in the direction perpendicular to both beams (vertical direction) was measured at each interaction energy with a slit probe moving through the center of the interaction region. Current profiles of the ions and electrons $I_i(z)$ and $I_e(z)$ were measured independently and numerical integration yielded the form factor F needed for determination of absolute cross sections

$$F = \frac{\int I_e(z)dz \int I_i(z)dz}{\int I_e(z)I_i(z)dz}. \quad (1)$$

The absolute cross sections are determined [22] from measured quantities using

$$\sigma(E) = \frac{R}{I_i I_e} \frac{qe^2 v_i v_e}{\sqrt{v_i^2 + v_e^2}} \frac{F}{\epsilon}, \quad (2)$$

where $\sigma(E)$ is the absolute cross section at the center-of-mass electron-impact energy E, R is the fragment signal rate, I_i and I_e are, respectively, the incident ion and electron currents, qe is the charge of the incident ions, v_i and v_e are the incident ion and electron velocities, F is the form factor that is determined from the two beam profiles, and ϵ is the channeltron detection efficiency for the product ions that we estimated to be 98% [23].

B. Ion beams

Since $^{12}CH_2^+$ has a mass of 14 amu, $^{14}N^+$ ions extracted from the ion source will not be separated and will be an impurity in our target beam. The fraction of N^+ ions in the beam is estimated from two sets of ionization data measured in the present study. First, using the crossed-beams apparatus, electron-impact ionization cross sections were measured at 100 eV for $m/q=14$ ions ($^{12}CH_2^+$ and N^+); both $^{12}CH_2^+$ and N^{2+} product ions were detected by the CEM. The ion source was cleaned to remove essentially all traces of carbon-12. Second, the ionization cross sections were measured for $^{13}CH_2^+$ using carbon-13 methane as the gas in the ECR ion source so that there would be no contamination from N^+ ions. The measured absolute cross sections are shown as the solid symbols in Fig. 2. Using the published cross section for ionization of N^+ at 100 eV [24], we determined the fraction of N^+ ions in the $m/q=14$ ion beam to be 4.8%. Since carbon-13 is only 1.1% of naturally occurring carbon, we estimate that the total amount of impurity ions in the $^{12}CH_2^+$ ion beam is less than 6%.

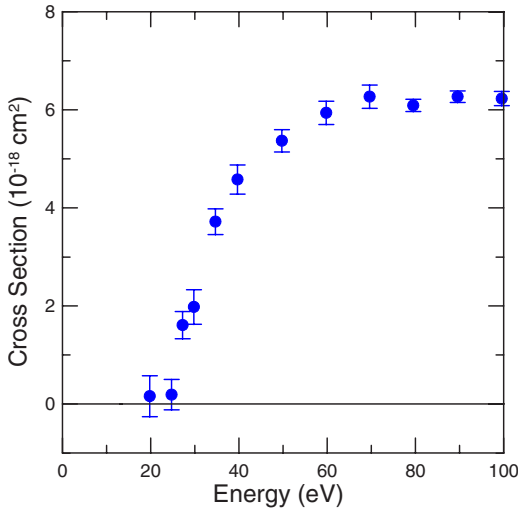

FIG. 2. (Color online) Absolute ionization cross sections for $^{13}CH_2^+$ as a function of center-of-mass energy. The filled circles are the present measurements shown with one standard deviation relative error bars.

Because the lifetimes of vibrational levels of the degenerate $CH_2^+(\tilde{X}\,^2A_1)$ and $CH_2^+(\tilde{A}\,^2B_1)$ ground states are on the order of 1 ms [25], much longer than the 1 μs flight time of the ions from the ECR source to the collision volume, the vibrational state population of the target CH_2^+ ions is essentially preserved from the ion source. In addition, there exists a metastable electronic state, CH_2^+ ($\tilde{a}\,^4A_2$), whose $v=0$ level lies about 3.7 eV above the ground state [26]. Even operating the source at minimal microwave power levels of a few watts and with source pressures of order 10^{-6} Torr, the electron temperature in the ECR discharge may be tens of eV or more, which we would expect to produce a sizable fraction of CH_2^+ ions in excited electronic and rovibrational states. The presence of excited vibrational states has been found to have a significant effect on measured cross sections for the dissociative recombination of CH^+ [27,28], although less dramatic influences are expected for DE and DI. We have no mechanisms for determining the fractions of low-lying excited states in the incident CH_2^+ ion beam, although whether these excited ions are present usually can be inferred from measurements below the lowest ground-state threshold. For CH_2^+ ions, however, no data exist for thresholds for the RDE processes, which likely possess the lowest thresholds for the CH^+ and C^+ fragment ion channels.

C. Collection and detection of fragment ions

Upon dissociation of a molecular ion, the fragments share KER that is the result of redistribution of the excess internal energy in the ion delivered in the collision with the electron.

Thus a given fragment will have a final velocity that is the vector sum of that of the target ion and a component due to its share of the KER. The maximum change in lab frame momentum occurs when the corresponding additional momentum Δp is parallel or antiparallel to the incident ion momentum P_0. In this case the dispersion of the fragment ion by the analyzing magnet causes a horizontal displacement Δx at the detector that is given by

$$\Delta x = D r_0 \frac{\Delta p}{p_0}, \tag{3}$$

where $p_0=(m/M)P_0$ is the fragment momentum for zero KER with parent and fragment masses M and m, respectively, r_0 is the ion orbit radius of curvature in the analyzing magnet, and D is the dispersion coefficient. For the present configuration, a double-focusing 90° sector magnet with entrance and exit angles of 26.5° and image and object distances of $2r_0$, the dispersion coefficient is 4 [29]. Applying conservation of energy and momentum to the fragmentation process, the maximum horizontal displacement is given by

$$\Delta x_{\max} = 4 r_0 \left(\frac{\Delta E}{E_i} \frac{M-m}{m} \right)^{1/2}, \tag{4}$$

where ΔE is the KER and E_i is the energy of the incident (parent) ion.

Measurements of the apparent dissociation cross section as a function of the analyzing magnetic field at a center-of-mass energy of 100 eV are shown in Fig. 3 for both the CH^+ and C^+ channels. The axes at the top of Fig. 3 indicate the distance that the center of the fragment ion peak is moved from the center of the detector by the analyzing magnetic field. As can be seen in Fig. 3(a), the CH^+ fragment ion peak can be moved 1.6 mm in either direction without any loss of apparent signal from the detector. At approximately 4.8 mm in either direction, one-half of the apparent signal is lost from the detector. From these two observations and noting that the radius of the CEM is 5.0 mm, one can infer that essentially all the signal is collected by the detector for a magnetic field of 2.83 kG and the maximum displacement $\Delta x_{\max}$ of the fragment ions from the center of the detector due to the effects of KER is 3.2 mm. Thus, an upper limit can be estimated for the average KER for dissociation of the CH_2^+ target ions producing CH^+ by using Eq. (4). Noting that $r_0=20$ cm for our analyzing magnet, one obtains an upper limit of 2.1 eV for the average KER. Janev and Reiter [6] estimate a mean total kinetic energy of 1.4 eV for the products of this DE channel. As seen in Fig. 3(b), the C^+ fragment ion peak cannot be displaced from the center position without loss of apparent signal, and the signal drops to essentially zero at one-detector-width displacement. These features imply that the signal is dispersed to the same size as the detector, i.e., $\Delta x_{\max}=5.0$ mm, yielding an upper limit of 2.5 eV for the average KER for dissociation of CH_2^+ into the C^+ fragment channel. Janev and Reiter [6] consider two DE channels leading to the C^+ fragment ion, which our experiment is unable to distinguish: $C^+ + H_2$ with an estimated mean total kinetic energy of 1.3 eV and $C^+ + H + H$ with an estimated mean total kinetic energy of 2.66 eV. Since our measured KER is much closer to the latter value, it seems the three-body channel ($C^+ + H + H$) may be the primary one; we note that dissociative recombination has also been shown to favor the three-body channel ($C + H + H$) for the CH_2^+ ion [11].

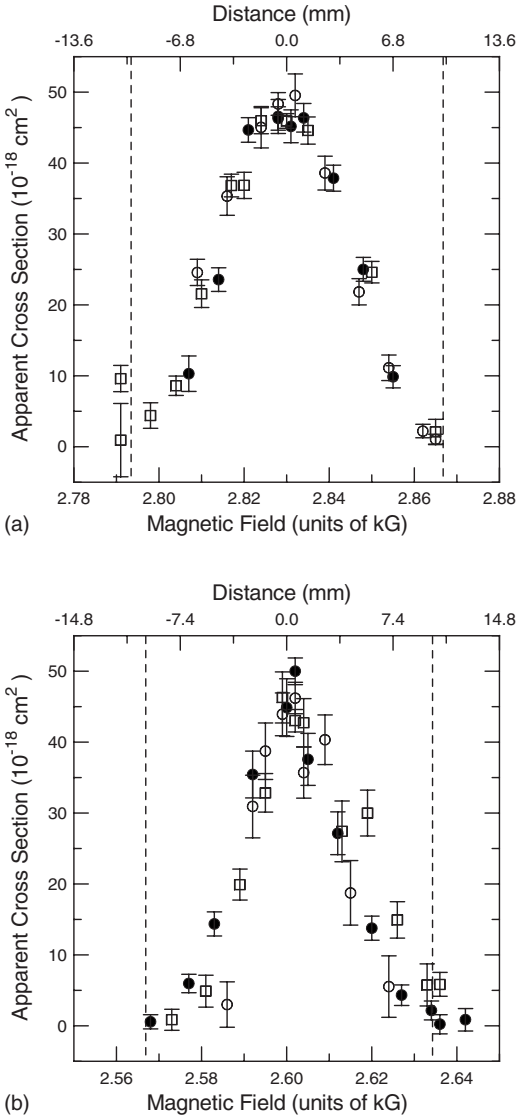

FIG. 3. Apparent cross sections for dissociation of CH_2^+ as a function of analyzing magnetic field. The measurements were made at a center-of-mass energy of 100 eV. The symbols depict three sets of measurements shown with one standard deviation relative error bars. The dashed vertical lines indicate the detector limits. (a) The CH^+ fragment ion channel and (b) the C^+ fragment ion channel.

The KER also causes angular spreading of the fragment ions, but this is mainly compensated by the double-focusing analyzer magnet. As demonstrated by trajectory modeling using the computer program SIMION [30], the spread of the fragment ions at the detector due to KER perpendicular to the target ion velocity is much smaller than that due to KER in the parallel direction. Note that angular spreading effects of KER are sufficient, however, to cause significant loss of H^+ and H_2^+ fragment ions, which are not collected in this experiment.

The voltage applied to the final vertical deflector that directs the CH^+ or C^+ fragment ions onto the CEM was also

scanned to test sensitivity and centering of fragment ions steered in this element. The apparent cross section did not change for variations of several hundred volts on either side of the value (8.5 kV) used for taking the present data.

High background count rates of 3–4 kHz/nA for the CH^+ fragment channel and 7–8 kHz/nA for the C^+ fragment channel, due to dissociation of the CH_2^+ ions on residual gas in the collision volume, necessitated limiting the incident ion current. By measuring the apparent cross section as a function of the total detector count rate, it was found that full signal could be maintained with count rates of 70 kHz, but increasing it beyond 100 kHz caused a reduction of greater than 10% due to reduced gain of the detector. Lowering the total count rate further, to below 20 kHz, did not yield any increase in the apparent cross section. Hence, most of the present data were obtained with ion currents limted to 15–20 nA for the CH^+ measurements and 7–9 nA for the C^+ measurements and ion count rates in the 50–65 kHz range. These limits were observed to minimize the time needed to reach a given statistical precision in the data while maintaining detector gain and limiting dead time corrections of the electronics to less than 7%.

The positions of the Faraday cups that collected the primary ion beam were optimized for each fragment channel to maintain the full current and signal while minimizing the ion background on the detector. Parameters for the electron chopping such as frequency, voltage, and delay times were also varied and found to have a negligible effect on the measured cross sections.

D. Uncertainties

The systematic uncertainties in the experiment arise from a number of sources connected to the measurement of the quantities in Eq. (2) and are given at a level equivalent to 90%-confidence level for statistical uncertainties. One contribution is from the detection of the C^+ and CH^+ fragment ions (estimated at 5%); this includes detection efficiency ϵ, pulse signal discrimination, and dead times of the detector and signal processing electronics. The transmission and collection of the fragment ions contributes an estimated 4% and includes possible losses due to fragment ions in the tail of the KER distribution. These two uncertainties are connected to the measurement of the true signal rate (R/ϵ) in Eq. (2). The systematic uncertainty of measuring the absolute form factor F is estimated to be 4%. Other contributions are from determinations of the ion current (6% including beam impurities), electron current (2%), and the ion and electron velocities (1% each). The quadrature sum of all these contributions is ±9.9%. Combining this sum with the statistical uncertainties at a 90%-confidence level yields the total expanded uncertainties for the measurements, typically about 11% near the cross section peak.

III. RESULTS

A. CH^+ fragments

Absolute cross sections for electron-impact dissociation of CH_2^+ ions producing the CH^+ fragment for energies up to 100 eV are shown in Fig. 4. The present measurements, the sum of the DE and DI channels, are indicated as filled circles and are shown with one standard deviation relative error bars, except for the point at 60 eV, where the outer set of error bars represents the total uncertainty of about 11% of the cross section in the flat portion of the curve above 30 eV.

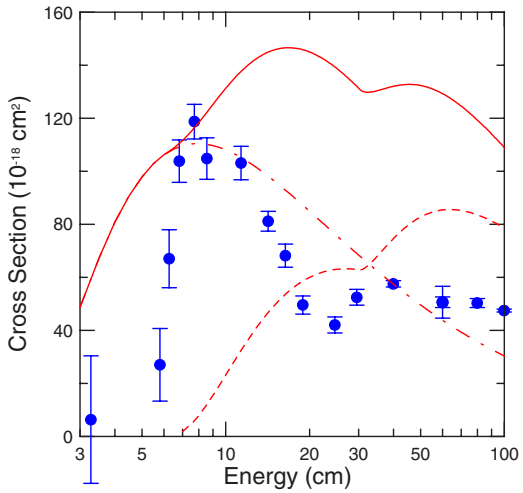

FIG. 4. (Color online) Absolute cross sections for the production of CH^+ fragment ions by electron-impact dissociation of CH_2^+ ions as a function of center-of-mass energy. The filled circles are the present measurements shown with one standard deviation relative error bars. The outer error bar at 60 eV represents the total uncertainty at a 90%-confidence level. The solid and dashed curves are estimates based on the formulation of Ref. [6]; see text for description.

The cross section rises sharply from an observed threshold of about 6 eV (this value is consistent with the DDE threshold of Janev and Reiter [6] given in Table I) and exhibits a strong peak in the 7–15 eV range, similar to that seen for the dissociation of DCO^+ [17]. For that ion, it was suggested that this peak feature is due to a series of strong vertical transitions to dissociative excited states. This process is analogous to excitation-autoionization in electron-impact ionization of atomic ions. Since potential energy curves for CH_2^+ are unavailable, we can only speculate that similar excitations may play a significant role in dissociation leading to CH^+ fragment ions in this energy range.

The empirical cross sections of Janev and Reiter [6] for the DDE and DI contributions are shown as the dashed curve in Fig. 4. Because of a lack of experimental data for CH_2^+, they do not provide any cross section estimates for the RDE process, which they refer to as capture assisted dissociation (CAD). The portion of this curve above 50 eV exceeds the measurements by about 60%, suggesting that their empirical formula overestimates the contribution of DI. Also shown in Fig. 4 is a solid curve that represents the DDE+DI contributions of Ref. [6] with an additional estimated RDE contribution. This contribution, shown as the dot-dashed curve in Fig. 4, is calculated using Eq. (20) of Ref. [6] with E_{th}=1.7 eV and using a constant multiplier of 7.0 instead of the 20.6 value they give. These values give approximately the correct magnitude and position for the peak in the 7–15 eV range, but clearly overestimate its width, suggesting that either the

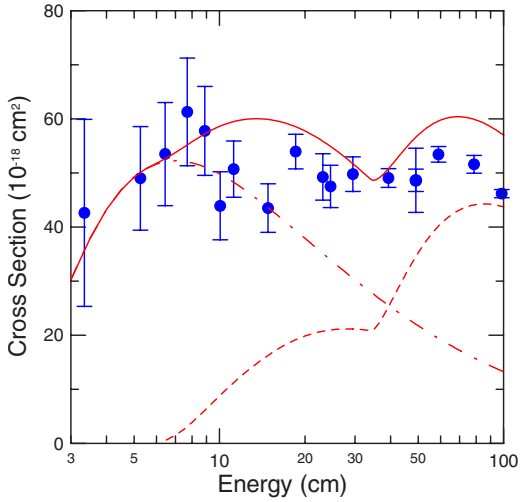

FIG. 5. (Color online) Absolute cross sections for the production of C^+ fragment ions by electron-impact dissociation of CH_2^+ ions as a function of center-of-mass energy. The filled circles are the present measurements shown with one standard deviation relative error bars. The outer error bar at 49 eV represents the total uncertainty at a 90%-confidence level. The solid and dashed curves are estimates based on the formulation of Ref. [6]; see text for description.

energy dependence is quite different than the form they give for RDE (CAD) or that this strong peak is not due to RDE processes. Since the observed threshold is about 6 eV, it is unlikely that the RDE process [6] makes a significant contribution to the CH^+ fragment ion channel. Above the DI threshold of 30.41 eV [6,31] the present measurements are the sum of the DE and DI channels producing CH^+ fragment ions, although no clear onset of the DI contribution can be seen in Fig. 4.

B. C^+ fragments

Absolute cross sections for electron-impact dissociation of CH_2^+ ions producing the C^+ fragment for energies up to 100 eV are shown in Fig. 5. The present measurements, the sum of the DE and DI channels, are indicated as filled circles and are shown with one standard deviation relative error bars, except for the point at 49 eV, where the outer set of error bars represents the total uncertainty of about 11% of the peak cross section.

In contrast to the results for the CH^+ fragment channel, the cross section for the C^+ fragment channel is relatively flat over the entire energy range of the measurements with no observed threshold. There appears to be a small peak near 8 eV with the cross section decreasing down to 3 eV, the lowest energy possible with the present electron gun. Extrapolation of this behavior yields a threshold of about 1 eV.

Also shown in Fig. 5 are empirical cross sections of Janev and Reiter [6] for the DDE+DI contributions; these are shown as the dashed curve. Their predictions clearly underestimate the experimental results, especially for energies below 50 eV. As was the case for the CH^+ fragment channel discussed above, they do not include RDE (CAD) contributions. The solid curve in Fig. 5 is a total cross section that includes an estimate of this RDE contribution (shown as the dot-dashed curve) calculated using Eq. (20) of Ref. [6] with $E_{th}=1.5$ eV and a constant multiplier of 3.0 instead of their value of 20.6. This gives reasonable overall agreement with the experimental results, although it appears that the DI contribution is again somewhat overestimated. The magnitude of the small peak near 8 eV is reproduced by their formula for RDE, and unlike the peak observed in the CH^+ fragment channel, the width is in good agreement with the measurements. This suggests that the weak peak in this C^+ fragment ion channel arises from a different physical mechanism than that producing the strong peak seen in the CH^+ channel.

Although no threshold is observed in Fig. 5 for the production of C^+ fragment ions, a threshold of about 1 eV can be inferred from extrapolation of the measurements at 8 eV and below. Since the lowest DDE threshold for producing C^+ is 5.62 eV (see Table I), this threshold is either the signature of RDE contributions from ground-state ions or of excited states present in the CH_2^+ ion beam. If the latter is true, then the excited states must preferentially dissociate via channels producing C^+ fragment ions because no dissociation signal was measured below the threshold for DDE of ground-state CH_2^+ ions for channels producing CH^+ fragment ions. It is more likely that the cross section measured below the DDE threshold is due to RDE processes with a threshold of about 1 eV. This conjecture is supported by the reasonable fit of RDE contributions estimated with the form of Janev and Reiter [6], as discussed above and shown in Fig. 5. Above the lowest DI threshold of 31.5 eV the present measurements are the sum of the DE and DI channels producing C^+ fragment ions, although only a slight increase in the cross section is seen in this region in Fig. 5.

C. Summary

It is interesting to note that the cross sections for the C^+ and CH^+ channels are practically identical for energies in the 15–100 eV range, despite the dramatic differences in the two channels below 15 eV. For the CH^+ channel, the cross section shows strong DDE contributions just above a threshold of about 6 eV. The C^+ channel, however, exhibits a low-energy dependence consistent with RDE contributions with a threshold of about 1 eV. Above 15 eV, both cross sections appear to be dominated by direct processes, including DI since the lowest DI thresholds for the CH^+ and C^+ channels are close.

In an effort to understand the total picture of electron-impact dissociation of CH_2^+ we compare the present results for (DE+DI) and ionization with published results for other dissociation channels; this is shown in Fig. 6 for energies in the 1–100 eV range. The solid circles and squares are the present (DE+DI) results, the open squares are the dissociative recombination (DR) measurements of Larson *et al.* [11], and the open circles are the (DE+DI) measurements of Djurić *et al.* [10] for the D^+ fragment channel. The light ion fragment DE measurements of Larson *et al.* [11] are in excellent agreement with those of Djurić *et al.* [10] and so are not shown in Fig. 6. Ionization of CH_2^+ is shown as the solid triangles. Note that in the 4–15 eV range, the heavy frag-

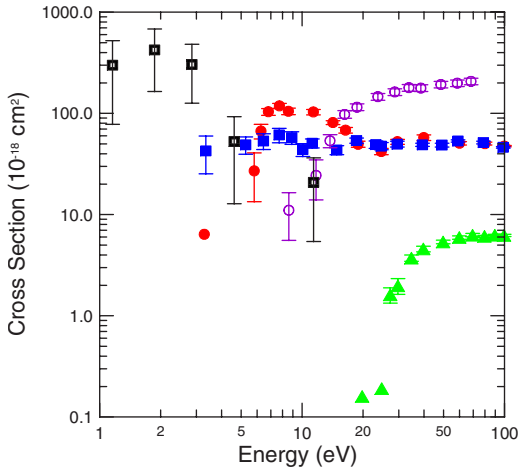

FIG. 6. (Color online) Absolute cross sections for the dissociation and ionization of CH_2^+ and CD_2^+ ions by electron-impact as a function of center-of-mass energy. The filled circles and squares are the present (DE+DI) measurements for the production of CH^+ and C^+ fragment ions, respectively, shown with one standard deviation relative error bars. The open circles represent the (DE+DI) measurements of Ref. [10] for the production of D^+ fragment ions. The solid triangles are present results for ionization of CH_2^+ and the open squares are the dissociative recombination measurements of Ref. [11].

ment ion (CH^+ and C^+) channels are dominant, although the production of H^+/D^+ fragments is the primary channel for higher energies. As expected, DR is the most important process below 2 eV.

IV. CONCLUSIONS

Absolute cross sections for electron-impact dissociation of CH_2^+ ions producing CH^+ and C^+ fragment ions have been measured employing the ORNL crossed-beams apparatus with a total expanded uncertainty of approximately 11% of the cross section in the flat portion of the curves above 30 eV. The dispersion pattern of the CH^+ and C^+ fragment ions in the analyzing magnetic field yields estimated upper limits of 2.1 and 2.5 eV, respectively, for the average KER at a collision energy of 100 eV. Because no other experimental or theoretical data exist for these dissociation channels, the present results are compared with the empirical cross sections of Janev and Reiter [6,12]. The agreement is reasonable for the C^+ fragment channel if an estimate of the RDE contribution is included; the agreement for the CH^+ is not nearly so good, partly because of a strong peak observed just above threshold in the 7–15 eV range that is not reproduced very well by their formulas for RDE and DDE contributions. The present data should serve as benchmarks for refining these empirical fits and hopefully stimulating theoretical investigations of these dissociation channels.

ACKNOWLEDGMENTS

This work was supported in part by the Office of Fusion Energy Sciences and the Office of Basic Energy Sciences of the U.S. Department of Energy under Contract No. DE-AC05-00OR22725 with UT-Battelle, LLC. E.M.B. gratefully acknowledges support from the ORNL Postdoctoral Research Associates Program administered jointly by the Oak Ridge Institute for Science and Education and Oak Ridge National Laboratory. R.D.T. acknowledges the support from the IHP program of the European Community (EC) under Contract No. HPRN-CT-2000-00142.

[1] H. Tawara, in *Atomic and Molecular Processes in Fusion Plasmas*, edited by R. K. Janev (Plenum, New York, 1995), pp. 461–496.
[2] R. K. Janev, T. Kato, and J. G. Wang, Phys. Plasmas **7**, 4364 (2000).
[3] A. Dalgarno, in *Atomic Processes and Applications*, edited by P. G. Burke and B. L. Moiseiwitsch (North-Holland, Amsterdam, 1976), pp. 109–132.
[4] J. Luque, W. Juchmann, E. A. Brinkman, and J. B. Jeffries, J. Vac. Sci. Technol. A **16**, 397 (1998).
[5] X. D. Zhu, R. J. Zhan, H. Y. Zhou, X. H. Wen, and D. Li, J. Vac. Sci. Technol. A **20**, 941 (2002).
[6] R. K. Janev and D. Reiter, *Collision Processes of Hydrocarbon Species in Hydrogen Plasmas: I. The Methane Family* (Forschungszentrum-Jülich, Jülich, Germany). Copies may be ordered from Forschungszentrum Jülich GmbH, Zentralbibliothek, D-52435 Jülich, Bundesrepublik Deutschland.
[7] W. Zong, G. H. Dunn, N. Djurić, M. Larsson, C. H. Greene, A. Al-Khalili, A. Neau, A. M. Derkatch, L. Vikor, W. Shi, A. Le Padellec, S. Rosén, H. Danared, and M. af Ugglas, Phys. Rev. Lett. **83**, 951 (1999).
[8] A. Le Padellec, N. Djurić, A. Al-Khalili, H. Danared, A. M. Derkatch, A. Neau, D. B. Popović, S. Rosén, J. Semaniak, R. Thomas, M. af Ugglas, W. Zong, and M. Larsson, Phys. Rev. A **64**, 012702 (2001).
[9] N. Djurić, G. H. Dunn, A. Al-Khalili, A. M. Derkatch, A. Neau, S. Rosén, W. Shi, L. Vikor, W. Zong, M. Larsson, A. Le Padellec, H. Danared, and M. af Ugglas, Phys. Rev. A **64**, 022713 (2001).
[10] N. Djurić, S. Zhou, G. H. Dunn, and M. E. Bannister, Phys. Rev. A **58**, 304 (1998).
[11] A. Larson, A. Le Padellec, J. Semaniak, C. Stromholm, M. Larsson, S. Rosén, R. Peverall, H. Danared, N. Djurić, G. H. Dunn, and S. Datz, Astrophys. J. **505**, 459 (1998).
[12] R. K. Janev and D. Reiter, Phys. Plasmas **9**, 4071 (2002).
[13] M. E. Bannister, Phys. Rev. A **54**, 1435 (1996).
[14] D. C. Gregory, F. W. Meyer, A. Müller, and P. Defrance, Phys. Rev. A **34**, 3657 (1986).
[15] P. A. Schulz, D. C. Gregory, F. W. Meyer, and R. A. Phaneuf, J. Chem. Phys. **85**, 3386 (1986).
[16] M. E. Bannister, H. F. Krause, C. R. Vane, N. Djurić, D. B. Popović, M. Stepanović, G. H. Dunn, Y.-S. Chung, A. C. H.

Smith, and B. Wallbank, Phys. Rev. A **68**, 042714 (2003).
[17] E. M. Bahati, R. D. Thomas, C. R. Vane, and M. E. Bannister, J. Phys. B **38**, 1645 (2005).
[18] F. W. Meyer, in *Trapping Highly Charged Ions: Fundamentals and Applications*, edited by J. Gillaspy (Nova Science Publishers, Huntington, NY, 2001), p. 117.
[19] P. A. Taylor and G. H. Dunn, Phys. Rev. A **8**, 2304 (1973).
[20] P. A. Taylor, K. T. Dolder, W. E. Kauppila, and G. H. Dunn, Rev. Sci. Instrum. **45**, 538 (1974).
[21] D. S. Belić, R. A. Falk, G. H. Dunn, D. Gregory, C. Cisneros, and D. H. Crandall, Bull. Am. Phys. Soc. **27**, 49 (1981).
[22] See, for example, M. F. A. Harrison, Br. J. Appl. Phys. **17**, 371 (1966).
[23] D. C. Gregory, P. F. Dittner, and D. H. Crandall, Phys. Rev. A **27**, 724 (1983).
[24] I. Yamada, A. Danjo, T. Hirayama, A. Matsumoto, S. Ohtani, H. Suzuki, T. Takayanagi, H. Tawara, K. Wakiya, and M. Yoshino, J. Phys. Soc. Jpn. **58**, 1585 (1989).
[25] A. Bear, Ph.D. thesis, Weizmann Institute of Science, Rehovot, Israel, 2000.
[26] N. R. Brinkmann, N. A. Richardson, S. S. Wesolowski, Y. Yamaguchi, and H. F. Schaefer III, Chem. Phys. Lett. **352**, 505 (2002).
[27] Z. Amitay, D. Zajfman, P. Forck, U. Hechtfischer, B. Seidel, M. Grieser, D. Habs, R. Repnow, D. Schwalm, and A. Wolf, Phys. Rev. A **54**, 4032 (1996).
[28] P. M. Mul, J. B. A. Mitchell, V. S. D'Angelo, P. Defrance, J. W. McGowan, and H. R. Froelich, J. Phys. B **14**, 1353 (1981).
[29] H. A. Enge, in *Focusing of Charged Particles*, edited by A. Septier (Academic Press, Orlando, 1967), Vol. II, Chap. 4.2, pp. 203–264.
[30] SIMION 3D, Version 6.0, David Dahl, INEL-95/0403, 1995.
[31] H. M. Rosenstock, K. Draxl, B. M. Steiner, and J. T. Herron, J. Phys. Chem. Ref. Data **6**, (Suppl. 1), 1 (1977).